JOURNAL OF GEOPHYSICAL RESEARCH, VOL. 113, B07102, doi:10.1029/2007JB005351, 2008

Physical property changes in hydrate-bearing sediment due to depressurization and subsequent repressurization

W. F. Waite,[1] T. J. Kneafsey,[2] W. J. Winters,[1] and D. H. Mason[1]

Received 28 August 2007; revised 21 February 2008; accepted 3 April 2008; published 3 July 2008.

[1] Physical property measurements of sediment cores containing natural gas hydrate are typically performed on material exposed, at least briefly, to non-in situ conditions during recovery. To examine the effects of a brief excursion from the gas-hydrate stability field, as can occur when pressure cores are transferred to pressurized storage vessels, we measured physical properties on laboratory-formed sand packs containing methane hydrate and methane pore gas. After depressurizing samples to atmospheric pressure, we repressurized them into the methane-hydrate stability field and remeasured their physical properties. Thermal conductivity, shear strength, acoustic compressional and shear wave amplitudes, and speeds of the original and depressurized/repressurized samples are compared. X–ray computed tomography images track how the gas-hydrate distribution changes in the hydrate-cemented sands owing to the depressurizaton/repressurization process. Because depressurization-induced property changes can be substantial and are not easily predicted, particularly in water-saturated, hydrate-bearing sediment, maintaining pressure and temperature conditions throughout the core recovery and measurement process is critical for using laboratory measurements to estimate in situ properties.

Citation: Waite, W. F., T. J. Kneafsey, W. J. Winters, and D. H. Mason (2008), Physical property changes in hydrate-bearing sediment due to depressurization and subsequent repressurization, *J. Geophys. Res.*, *113*, B07102, doi:10.1029/2007JB005351.

1. Introduction

[2] Pressures and temperatures in continental margin and permafrost sediments can stabilize gas hydrate, a crystalline solid in which hydrogen-bonded water molecules enclose individual guest molecules [*Kvenvolden and Lorenson*, 2001]. The most common guest molecule in naturally occurring gas hydrate is methane. Hydrate-bound methane represents a potential energy resource [*Kerr*, 2004; *Ruppel*, 2007], and may play a role as a greenhouse gas in the global climate [*Kvenvolden*, 1993]. Sediment weakening caused by gas-hydrate dissociation has the potential to cause submarine slumps or slides, endangering seafloor infrastructure [*Hovland and Gudmestad*, 2001; *Nixon and Grozic*, 2007].

[3] Interest in methane hydrates has motivated several large-scale field efforts to recover and study hydrate-bearing sediment from marine environments and beneath permafrost. Pressure coring systems represent a significant advance toward recovering pristine cores from which to infer in situ physical property values. The Fugro and HYACE systems used aboard Ocean Drilling Program (ODP) Leg 204 [*Leg 204 Shipboard Scientific Party*, 2003] and International Ocean Drilling Program (IODP) Expedition 311 [*Expedition 311 Scientists*, 2006] are designed to retrieve and preserve meter-long core samples near their in situ hydrostatic stress. Although some physical property testing can be accomplished without ever releasing the hydrostatic stress [*Yun et al.*, 2006], specialized measurements, such as triaxial shear-strength tests, are not yet possible without a brief hydrostatic stress release.

[4] To accommodate these and other laboratory tests, pressure cores containing hydrate-bearing sediment have been rapidly subsectioned and transferred at one atmosphere to storage and transfer vessels, in which they are subsequently repressurized and stabilized with methane gas [*Collett et al.*, 2006; *Expedition 311 Scientists*, 2006]. This process takes approximately 5 min to complete (P. Schultheiss, personal communication, 2007).

[5] Pressure cores containing hydrate-bearing sediment have also been subsectioned and transferred into storage and transfer vessels through ball valves, which allow the process to be completed with almost no loss of hydrostatic pressure [*Collett et al.*, 2006; *Winters et al.*, 2005]. Although core manipulation and measurement systems can be designed and built to accommodate sample transfers, many existing laboratory systems have not been designed with this capability. For some measurements, pressurized transfer may never be possible. In such cases, samples must undergo a one-atmosphere transfer to the laboratory apparatus prior to repressurization and the measurement of physical properties. In this work, we focus primarily on effects from a single one-atmosphere transfer, though we also consider a case involving a second transfer, as would be required to transfer material from a storage vessel into some laboratory systems.

[6] Rapidly venting a pressure core stored above 0°C to atmospheric pressure exposes the core to pressure well

[1] U. S. Geological Survey, Woods Hole, Massachusetts, USA.
[2] Lawrence Berkeley National Laboratory, Berkeley, California, USA.

Table 1. Porosity ϕ and Pore-Space Hydrate Saturation S_h of Hydrate-Bearing Ottawa Sands in This Study Prior to the Brief Depressurization[a]

Sample	ϕ, %	S_h, %
CT 1	38	35
Thermal 1	37	20
Thermal 2	42	34
GHASTLI 1	37	20
GHASTLI 1a	38	19
GHASTLI 2, 2a	37	43

[a]Remaining pore space contains pressurized methane gas. Full conversion of pore water to methane hydrate is assumed for all samples except CT 1, which contains a 14.5% pore-space saturation of residual water in addition to methane hydrate. GHASTLI samples 1a and 2a were not subjected to a brief depressurization. Uncertainties are ±4%.

below the hydrate stability pressure, inducing hydrate dissociation and gas bubble formation. Repressurization with methane once the subsectioned sample is placed in a storage and transfer vessel stabilizes hydrate remaining in the sample, but also provides gas for additional hydrate formation. The net effect of such a transfer on the distribution of water, gas and hydrate within a core and the corresponding changes in the core's physical properties must be evaluated to determine whether measurements on disturbed core provide values representative of the undisturbed core.

[7] To limit hydrate dissociation, cores have also been frozen prior to depressurization, or have been depressurized and subsequently stored in liquid nitrogen at atmospheric pressure. Though hydrate dissociates more slowly when depressurized below 0°C [*Stern et al.*, 2001], pore water expansion during the freezing process can generate a network of cracks that significantly disturb the sediment fabric. We discuss these effects in section 5 with regard to recovering natural core material, but our laboratory work is focused on unfrozen material.

[8] To examine the alteration of hydrate-bearing sediment that undergoes hydrate dissociation caused by sample depressurization above 0°C and subsequent hydrate formation following sample repressurization, we measured physical properties of methane hydrate-cemented sands formed in the laboratory. As discussed in section 3, X−ray computed tomography (CT) imagery, thermal conductivity, shear strength, acoustic compressional and shear wave speeds and amplitudes were measured first on undisturbed hydrate-cemented sand samples, and then again after the samples equilibrated following a brief exposure to atmospheric pressure. These results are presented in section 4.

[9] By construction, our laboratory samples were combinations of sand, methane hydrate, water and free methane gas, formed in the presence of free gas as discussed in section 2. Naturally occurring hydrate formed in the presence of free gas is thought to occur in the shallow sediments of actively venting regions such as the Cascadia margin [*Bohrmann et al.*, 1998], and at the base of the hydrate stability zone where gas can be recycled into the hydrate stability field [*Guerin et al.*, 1999; *Yuan et al.*, 1999].

[10] The extent to which hydrate cements sediment grains is still debated, even with regard to studies of a single site [*Guerin and Goldberg*, 2005; *Lee and Collett*, 2005], but the strong intergranular bonding observed in our laboratory-formed samples is analogous to the bonding observed highly hydrate-saturated sands [*Yun et al.*, 2007]. Sands containing pore-space hydrate saturations exceeding 50% have been found in permafrost [*Lee and Collett*, 1999, 2005; *Mount Elbert Science Team*, 2007] and marine settings [*Matsumoto*, 2002; *Smith et al.*, 2006], and represent potential resource targets. We discuss connections between our laboratory observations and the behavior of highly hydrate-saturated sands in section 5.

[11] In sediment with lower hydrate saturations, particularly in fine-grained sediment, a brief depressurization can alter sediment physical properties via gas bubble formation and effective stress loss [*Yun et al.*, 2006] in addition to the hydrate redistribution we observe in our laboratory samples. These processes are discussed in section 6.

2. Sample Preparation

[12] We created samples containing quartz sand, methane hydrate and methane gas in the pore space. The hydrate-bearing sand samples were all formed according to a single procedure for the physical property measurements conducted at the U.S. Geological Survey facility in Massachusetts and the CT scanning experiments carried out at Lawrence Berkeley National Laboratory in California. Samples were not transferred between institutions.

[13] Ottawa sand with a grain size range of 50−300 μm for the CT scanning and 250−500 μm for the physical property testing, was premixed with water, adding water in steps until the desired initial water content was reached. Samples were formed by tamping ~1cm lifts of the sand+water mixture into the measurement vessel. This packing process produced samples with ~38% porosity, as determined from the overall sample volume and mass of sand and water used. Sample-specific porosities and initial water saturations are given in Table 1. The choice of quartz grain size represents the on-site availability, not intrinsic requirements of either the CT or physical property measurement systems.

[14] Samples were then pressurized with methane gas and cooled into the hydrate-stability field. Hydrate formation was allowed to continue until the formation rate became insignificant. Apparatus-specific measurements, described below, were used to determine when the sample was equilibrated, so the formation times differ between systems. Hydrate formed in this fashion within gas-rich, water-limited samples surrounds and cements sediment grains [*Waite et al.*, 2004].

[15] The one-atmosphere transfer was simulated by depressurizing to one atmosphere, then repressurizing using methane gas. The sample was then allowed to re-equilibrate until the hydrate formation rate became insignificant. Timing for the depressurization and repressurization steps was guided by the 5-min transfer accomplished in the field. In practice however, depressurization and repressurization rates were limited by the complexity of the laboratory instrument used, and therefore varied from system to system as noted below.

3. Measurement Technique

[16] Three separate systems were used to assess the effects of a brief depressurization on hydrate-bearing sands.

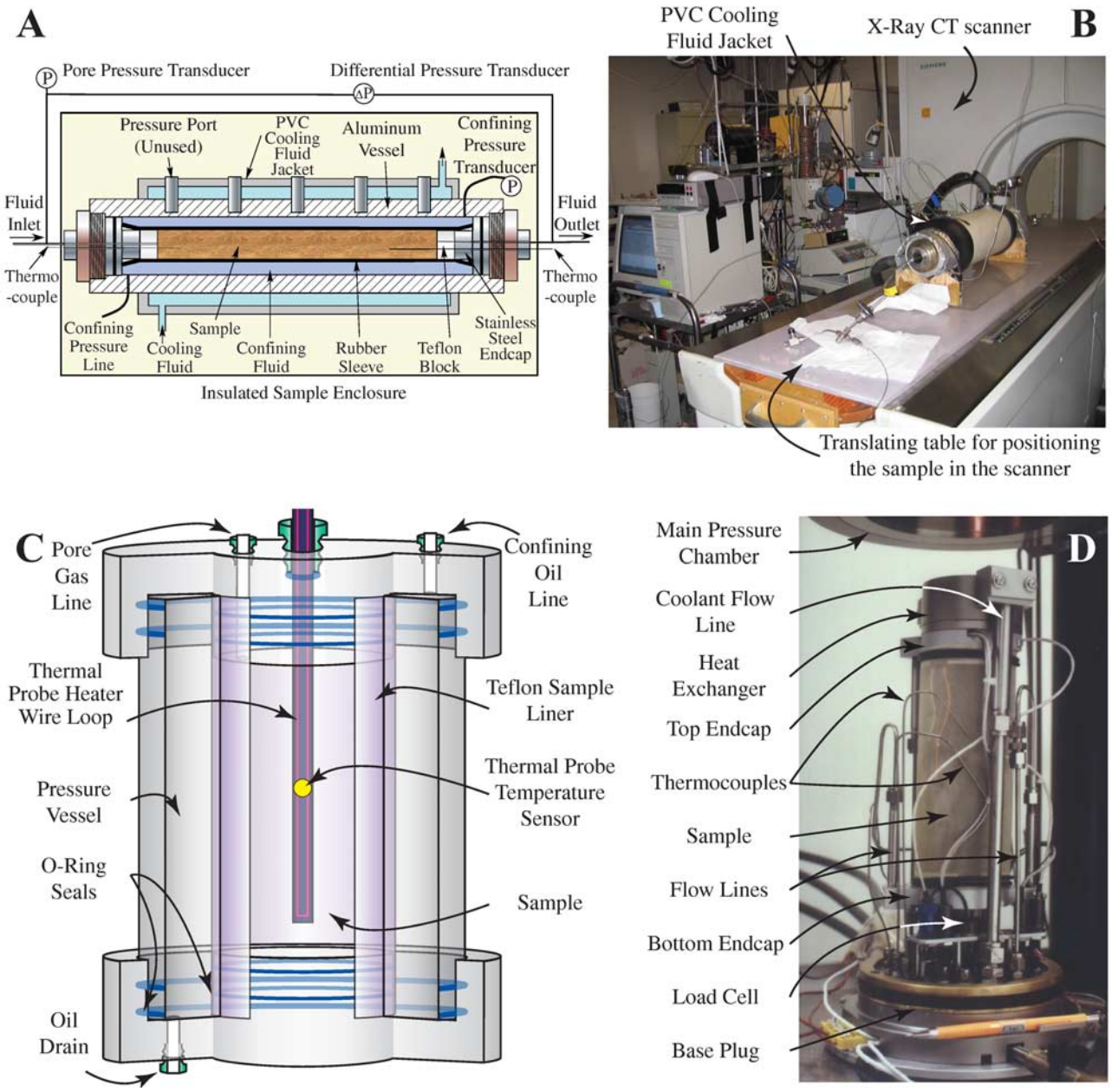

Figure 1. (a) Schematic of the X–ray computed tomography (CT) sample vessel. The sample is 37 cm long, by 5 cm in diameter. (b) The CT sample vessel and surrounding temperature control bath are positioned in the X–ray CT scanner using a translating table. (c) Cutaway schematic of the thermal conductivity pressure vessel. Cylindrical hydrate samples 13.3 cm long by 4.1 cm in diameter are formed around a thermal probe (enlarged to show detail). (d) View of a 14-cm-long, 7-cm-diameter sample prior to raising the sample up into the main pressure chamber of the Gas Hydrate and Sediment Test Laboratory Instrument (GHASTLI). Acoustic measurements are made using axially positioned sensors in the top and bottom endcaps. Shear-strength measurements are made by axially straining the sample using a ram brought into contact with the heat exchanger. The load supported by the sample during shear is measured by the load cell beneath the sample.

Schematics for all three systems are given in Figure 1, with details of their use given below.

3.1. X–ray Computed Tomography

[17] CT was used to map the initial hydrate distribution as well as the hydrate distribution within the cemented sand resulting from a simulated one-atmosphere transfer. A complete description of the CT imaging technique is given by *Kneafsey et al.* [2007]. To summarize, CT images were collected using a modified Siemens HiQ medical X–ray computed tomography scanner (Figure 1b), scanning 0.5 cm slices over the length of the sample (Figure 1a). A CT image captures the sample density, with a resolution given by the voxel size. For scans shown here, the voxel size was 0.25 ×

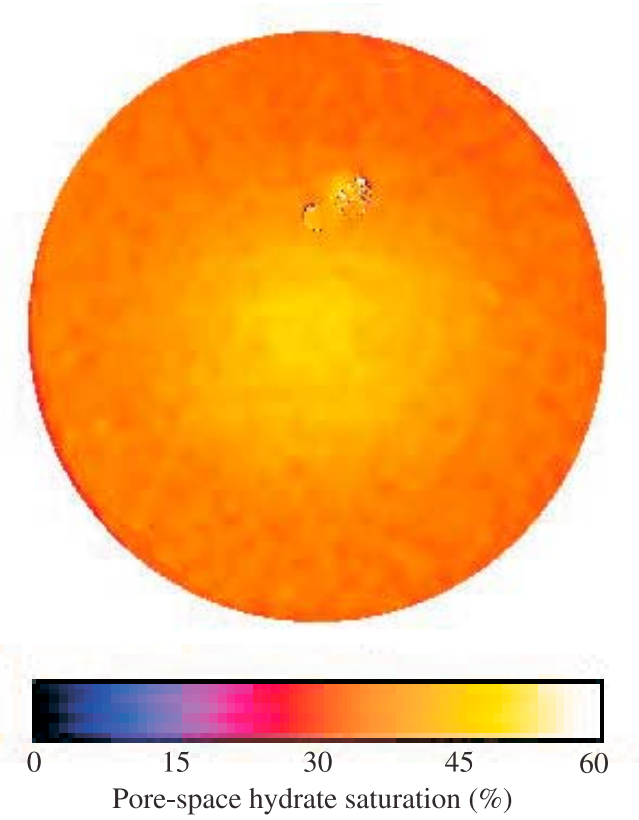

Figure 2. Cross section of a methane-hydrate-cemented quartz sand containing methane gas in the pore space. The picture represents the average of 56 CT scans along the length of the sample. The pore-space hydrate saturation ranges from 26 to 46%, with an average of 35 ± 4%. Speckling in the center top portion of the scan is caused by thermocouples embedded in the sample.

0.25 × 5 mm. The 5-cm-diameter, 37-cm-long cylindrical sample was jacketed in a rubber sleeve and surrounded by confining fluid in a pressure vessel. The pressure vessel itself was housed in a temperature-controlled PVC jacket and placed in an insulating box.

[18] Methane hydrate was initially formed in sample CT 1 (see Table 1) at approximately 4°C and 5.2 MPa methane pore pressure. After 20 h, the sample was scanned to obtain the initial gas-hydrate distribution. From mass balance, it was determined that ~67% of the initial pore water had converted to hydrate. The average pore-space hydrate saturation was 35±4%, with hydrate saturations ranging from 26% near the sample perimeter to 46% near the sample's axis (Figure 2). The sample was then depressurized over the course of 10 min, held at atmospheric pressure for 6 min, then repressurized over a 10-min period. The sample was out of the methane-hydrate stability field for 19 min. CT scans were taken 1.66 and 24 h after repressurization was completed. Measured density changes in the sample before and after the simulated one-atmosphere transfer reflect both the redistribution of methane hydrate and any additional hydrate growth from previously unreacted water.

3.2. Thermal Conductivity λ

[19] Thermal conductivity is a measure of how easily heat travels through a material. We measured λ using an axially positioned probe in a 41-mm-diameter, 133-mm-long cylindrical sample as described by *Waite et al.* [2006]. The measurement vessel is shown schematically in Figure 1c. A resistive wire in the probe heats the sample, and λ is calculated from the temperature change measured by a thermistor in the probe. The uncertainty in our thermal conductivity measurements is conservatively estimated to be ±1% [*Waite et al.*, 2006]. In a sand containing gas, λ is sensitive to the pore-space hydrate saturation [*Waite et al.*, 2002] and can be expected to change in response to a redistribution of hydrate around the thermistor.

[20] Two pore-space hydrate saturations were tested for thermal conductivity changes during a simulated one-atmosphere core transfer. Characteristics of samples Thermal 1 and 2 are given in Table 1. Methane hydrate was formed at 5°C and 12 MPa methane pore pressure from initially partially water-saturated sand. The confining pressure balanced the pore pressure, meaning the samples experienced no effective stress. After 11 days, the measured λ showed no further change, and hydrate formation was deemed complete. Sample conditions were changed to 6.1°C and 12 MPa methane pore pressure and allowed to equilibrate overnight at the test conditions used in the acoustic and strength measurements described below.

[21] The simulated one-atmosphere transfer was carried out by dropping the pore and confining pressures to atmospheric pressure over a 1-min period. Three minutes later, the pore and confining pressures were increased to 12 MPa over 1 min. To examine the effects of a second one-atmosphere transfer, as would occur if a core were transferred out of a storage vessel and into a laboratory system, a second depressurization/repressurization cycle was carried out, 7 days after the first simulated transfer.

3.3. Acoustic Wave Speed

[22] Compressional and shear waves contain information about the rigidity of grain-to-grain contacts, which in turn is affected by the extent to which hydrate binds grains together [*Helgerud et al.*, 1999]. We used the Gas Hydrate and Sediment Test Laboratory Instrument (GHASTLI), described by *Winters et al.* [2000], to perform compressional and shear wave analysis on methane-hydrate-cemented sands containing two different pore-space hydrate saturations (GHASTLI 1, 1a, 2, and 2a in Table 1). As with the thermal property samples, the remaining pore space was filled with pressurized methane gas.

[23] Cylindrical samples approximately 14 cm high and 7 cm in diameter were prepared as described above by tamping premixed, wet sand into a flexible liner, subsequently capped at each end by a metal endcap. Figure 1d shows a prepared sample, ready to be raised into the GHASTLI pressure chamber.

[24] The endcaps house axially positioned, 1 MHz compressional and shear wave transducers. Acoustic waves were produced in the top endcap and were detected by the transducer crystal in the bottom endcap. Wave speed was calculated by dividing the acoustic travel time through the sample by the sample length, as measured using a linear voltage displacement transducer. The acoustic wave speed

Table 2. Physical Property Changes in Methane-Hydrate-Cemented Sands Resulting From a Brief Depressurization to One Atmosphere, Followed by a Repressurization Into the Methane-Hydrate Stability Field[a]

Property	Porosity, %	S_h, %	Initial Value	Final Value	Change, %	Uncertainty, %
λ	37	20	1.67 W/(m K)	1.76 W/(m K)	5.4	±1
λ	42	34	1.60 W/(m K)	1.82 W/(m K)	13.8	±1
V_p	37	20	2830 m/s	2960 m/s	4.5	±0.5
V_p	37	43	3430 m/s	3350 m/s	−2.4	±0.5
V_s	37	20	1580 m/s	1770 m/s	11.7	±3
V_s	37	43	1320 m/s	1945 m/s	47.0	±3
S_u	37/38[b]	20/19[b]	2.31 MPa	1.89 MPa	−18	±15
S_u	37	43	2.94 MPa	2.81 MPa	−4.5	±15

[a]Measured properties include thermal conductivity λ, compressional and shear wave speeds, V_p and V_s, respectively, and triaxial undrained shear strength S_u.

[b]The two samples required for undrained shear strength differed slightly in their initial porosity and hydrate saturation S_h (see Table 1).

uncertainty is ±0.5% for compressional wave speeds, V_p [*Waite et al.*, 2004]. Because of uncertainties in choosing the shear wave arrival, the uncertainty in the shear wave speed, V_s, is conservatively estimated to be ±3%.

[25] In the GHASTLI pressure vessel, the sample's methane pore pressure, controlled by a syringe pump connected through a line in the endcap, was held at 12 MPa while the temperature was lowered from room temperature and held at 6.1°C. The independently controlled confining pressure was held via syringe pump at 12.25 MPa to impart an effective pressure of 250 kPa. As hydrate formed in the sample, the acoustic signal increased in amplitude and the measured wave speed increased [*Waite et al.*, 2004]. Hydrate formation was deemed complete when the acoustic amplitude and measured wave speed stabilized, 5 days after onset of hydrate formation for the low-saturation sample, 14 days for the higher-saturation sample.

[26] To simulate a one-atmosphere core transfer, we reduced the pore pressure and confining pressure together over the course of 3 min, held them at atmospheric pressure for 1.5 min, and repressurized them over the course of 5.5 min. The samples were out of the methane-hydrate stability field for 7.5 min. They were then allowed to equilibrate at the original formation conditions until the acoustic signal restabilized, which took 2 days for the low-hydrate-saturation sample, and 3 days for the high-hydrate-saturation sample.

3.4. Shear Strength

[27] Triaxial shear-strength measurements provide a means of assessing sediment stability. In hydrate-bearing sediment, strength loss resulting from hydrate dissociation can cause localized failures in drilling and seafloor pipeline applications [*Hovland and Gudmestad*, 2001; *Moridis and Kowalsky*, 2006], or regional-scale slope failure [*Paull et al.*, 2000]. Undrained shear strength was measured by using a ram to axially strain the sample while the confining pressure, pore pressure, and load supported by the sample were recorded. The ram extended at a constant 5.6 mm/h, equivalent to an initial strain rate of 4.4%/h. We ran the shear-strength test in the undrained configuration, meaning the pore space was isolated and the pore pressure changed as the sample length decreased.

[28] Unlike the other property measurements described here, shear-strength measurements are destructive and therefore cannot be carried out on a single sample both before and after a simulated one-atmosphere transfer. We estimate the effect of a one-atmosphere transfer on shear strength by comparing the shear strength for samples GHASTLI 1 and 2, which undergo the transfer procedure, with nominally identical samples that do not undergo the simulated one-atmosphere transfer (GHASTLI 1a and 2a in Table 1). Shear-strength measurement uncertainties in hydrate-bearing sediment are difficult to quantify because shear strength depends sensitively on how sediment grains are packed, the extent to which they are interlocked, and their degree of cementation [*Bowles*, 1979] Difficulties in precisely replicating the distribution and sediment bonding by methane hydrate increases sample-to-sample variations in shear strength. Extensive work by *Hyodo et al.* [2005] on laboratory-formed mixtures of methane hydrate and sediment suggests uncertainties of ±15% are to be expected.

4. Laboratory Results for Gas-Rich, Methane Hydrate-Bearing Sediment

[29] In a one-atmosphere transfer, methane-hydrate-cemented sediment first undergoes a depressurization-induced dissociation that can disrupt or destroy the sediment fabric and radically alter a range of physical properties [*Francisca et al.*, 2005]. Subsequent hydrate formation following repressurization will not likely restore all of the sample's physical properties, particularly if the initial and final hydrate distributions differ.

[30] Here we look at the net physical property changes resulting from a brief pressure excursion to one atmosphere. Conclusions are drawn by comparing measurements on a given sample before and after a brief depressurization, meaning sample-to-sample variations are not responsible for the observed property changes. The exception is the undrained shear strength, S_u, which as noted previously, requires a destructive test of two samples to evaluate the effects of a brief depressurization. Sample-to-sample variability increases the S_u analysis uncertainty relative to the other measured properties (see Table 2). Following the discussion of property changes resulting from a brief depressurization, we comment in section 4.5 on the dependence of the sample's initial physical properties on hydrate saturation.

4.1. X−ray Computed Tomography

[31] Density changes resulting from the simulated core retrieval process were observed in CT images taken 1.66 and ~24 h after briefly depressurizing the sample. Figure 3a is a cross section of sample C1 showing the average density change 1.66 h after the simulated core transfer, relative to the sample density after the initial hydrate formation. Figure 3b shows the average density change measured ~24 h after the depressurization/repressurization procedure, relative to the sample density after the initial hydrate formation. The density changes are small enough that, in spite of the constant level of measurement noise, speckling is more apparent in the density difference profiles shown in Figure 3 than in the sample density profile shown in Figure 2.

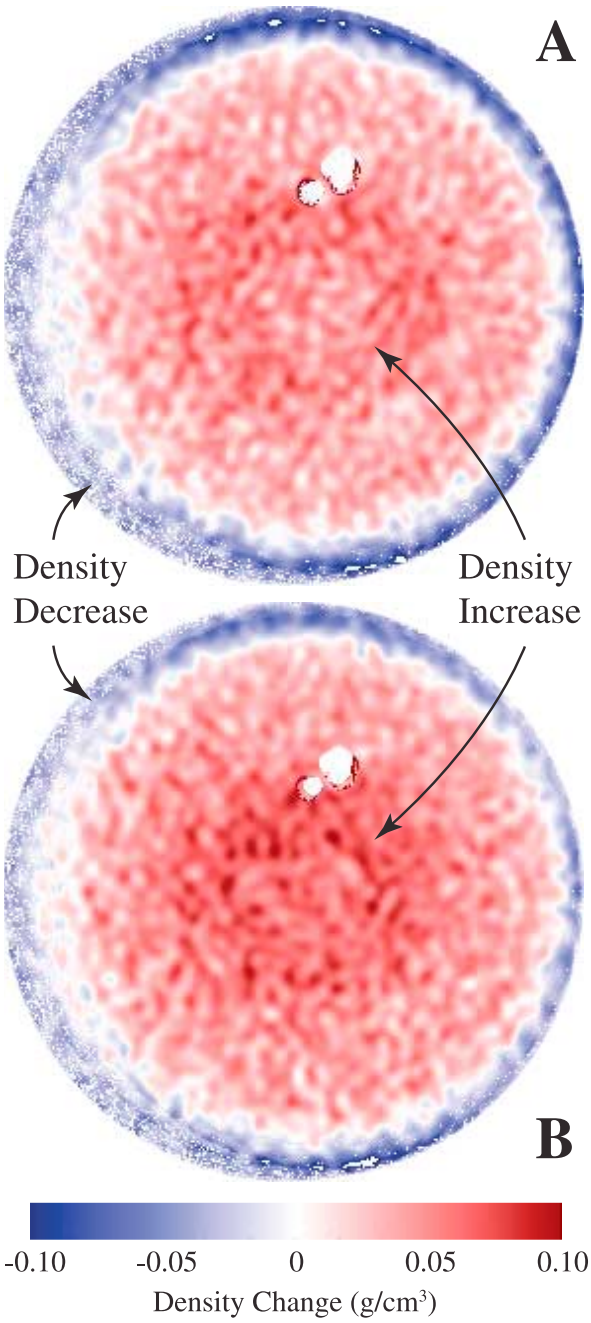

Figure 3. Density change in a methane-hydrate-cemented quartz sand as a result of a brief depressurization to one atmosphere and subsequent repressurization with methane gas. The picture represents the average of 56 CT scans along the length of the sample. (a) Hydrate reforms rapidly, measurably increasing the density near the central sample axis, while decreasing the density near the sample surface within 1.66 h of repressurization. (b) The redistribution pattern becomes more accentuated ~24 h after repressurization. White holes in the center top portion of both scans are thermocouples embedded in the sample.

[32] Figure 3 shows the average over 56 of the 78 scanned sections of the sample. The remaining 22 sections contained serious scanning artifacts that rendered them unusable in this study. In any given slice, measurement noise tends to obscure the hydrate-redistribution pattern, but a sensitivity analysis shows that density changes exceeding 0.01 g/cm^3 observed in regions of 0.04 cm^2 in the averaged cross section have nearly a 90% level of confidence and can be considered real. The white holes in the center top of the cross section are from thermocouples embedded in the sample. The speckled pattern on the left side of Figure 3 results from averaging scans down the length of a sample with a slightly nonuniform diameter.

[33] As discussed in section 4.5, capillary action can cause water to migrate during the initial hydrate formation, leading to the radial inhomogeneity observed in Figure 1 prior to the brief depressurization. The initial density distribution is not responsible for the density change pattern resulting from the brief depressurization, however. Because the density change profiles shown in Figure 3 are the density difference between the postdepressurization and predepressurization densities, the initial sample's inhomogeneities are removed. Both the density increase near the sample's central axis, and the observed decrease at the sample's perimeter represent sample inhomogeneity caused by the brief depressurization.

[34] A density increase near the sample's central axis, combined with a density decrease observed at the sample perimeter, can be explained by a net inward migration of material. We propose the hydrate redistribution process illustrated in Figure 4 accounts for much of the observed density change. Figure 4a represents a cross section of an essentially uniform distribution of sand grains, methane hydrate and methane gas. Depressurizing the sample destabilizes the hydrate, which begins dissociating to methane gas and water (Figure 4b). Hydrate dissociation is endothermic, and because the surrounding bath provides the most readily available heat source to fuel dissociation, dissociation initially occurs most efficiently on the outer sample perimeter. Time-lapse CT imagery during hydrate dissociation shows the dissociation front propagates toward the central axis of the sample over time [*Kneafsey et al.*, 2007].

[35] The sample is repressurized with methane gas before the dissociation front reaches the sample's central axis. Hydrate persisting near the sample's central axis forms a surface for rapid growth of new hydrate following the repressurization step [*Osegovic et al.*, 2006]. Capillary forces draw water to the hydrate formation front [*Gupta et al.*, 2006; *Kneafsey et al.*, 2007] (Figure 4c), reducing the water available for hydrate formation near the sample perimeter. Overall, the process increases the pore-space hydrate saturation near the sample's central axis, while reducing the hydrate saturation near the sample's perimeter (Figures 3 and 4d).

[36] Two additional hydrate formation processes contribute to the density increase near the sample's central axis, though as shown below, neither process can account for the density decrease at the sample perimeter. The two processes are as follows: (1) new hydrate formation from water that had not yet formed hydrate just prior to the brief depressurization and (2) hydrate formation from water that does not migrate during the brief depressurization.

[37] Prior to the brief depressurization of sample C1, approximately 67% of the initial water was thought to have been converted to hydrate. Depressurization can crack

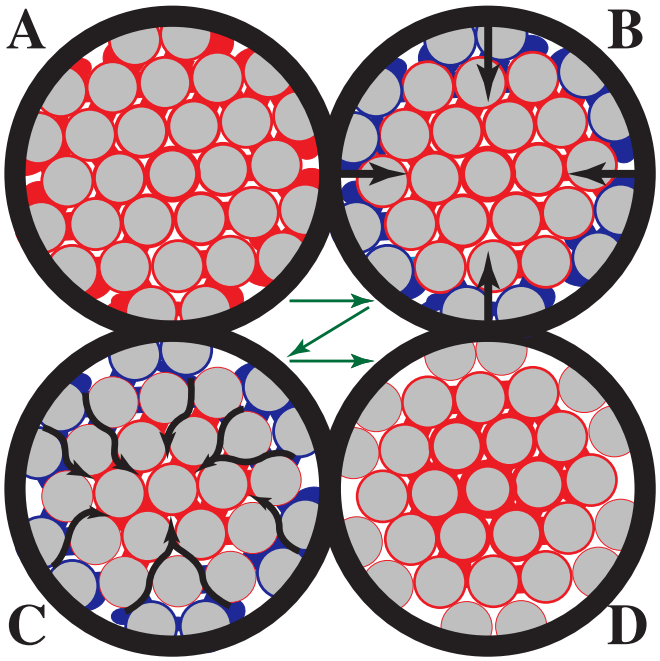

Figure 4. Cross-sectional schematic (not to scale) of methane-hydrate redistribution in a quartz sand (grey circles) during a depressurization and subsequent repressurization with methane gas. (a) Initially, methane hydrate (red) and methane gas (white) are fairly uniformly distributed. (b) Depressurization induces hydrate dissociation to water (dark blue) and methane gas. Dissociation front moves inward (black arrows) as heat is supplied from the surrounding bath. (c) Hydrate growth following repressurization is most efficient where hydrate persists, drawing water inward via capillary action (black arrows). (d) Final hydrate distribution is concentrated near the sample's central axis and depleted near the sample perimeter.

hydrate layers that isolated portions of the remaining initial water volume from the surrounding methane gas [*Kneafsey et al.*, 2007]. Subsequent repressurization exposes methane gas to that previously unreacted water, allowing new hydrate growth. This growth is in addition to growth from water liberated via hydrate dissociation during the brief depressurization. The volume increase associated with converting a volume of water to gas hydrate in sands at these pressures means low-density methane pore gas is replaced by higher-density hydrate, resulting in a net density increase.

[38] Because the water/methane interface is an active hydrate growth zone, a portion of the available water likely forms hydrate in place, without first migrating toward the sample's central axis. Hydrate forming in place from water liberated during dissociation returns the local density to predepressurization levels, resulting in no net density change. Hydrate forming in place from previously unreacted water increases the sample density everywhere it occurs. The relative contribution of this mechanism to the observed density increase near the sample's central axis is not known, but this mechanism has been observed in CT scans of similar samples in which the pore gas pressure was changed, but remained within the methane-hydrate stability field [*Kneafsey et al.*, 2007]. Without water migration resulting from the brief depressurization, however, hydrate formation following the brief depressurization cannot cause the density decrease noted at the sample's perimeter in Figure 3.

[39] We attribute the observed density changes induced by a brief depressurization to a combination of hydrate growth from water that has migrated toward the sample's central axis, in place hydrate regrowth from water liberated from hydrate during the depressurization, and new hydrate growth from previously unreacted water.

[40] As we show in sections 4.1–4.5, physical property changes resulting from a brief depressurization of gas-rich, hydrate-bearing sand vary with the initial hydrate content, the amount of unreacted water prior to depressurization, and pore-size-dependent capillary forces. We therefore use the CT results to visualize hydrate redistribution, but not to predict the magnitude of physical property changes occurring in other gas-rich, hydrate-bearing sands as a result of hydrate redistribution.

4.2. Effect on Thermal Conductivity Measurements

[41] Because we measure λ using an axially positioned probe, our measurement is most sensitive to changes occurring near the sample's central axis. The hydrate redistribution observed in the CT scans should increase the measured λ for two reasons: (1) λ of methane hydrate is $\sim$0.62 W/(m K) [*Waite et al.*, 2007], more than an order of magnitude larger than that of the methane gas (0.045 W/(m K) [*Vargaftik et al.*, 1993]) being replaced by hydrate, and (2) methane hydrate provides a more efficient thermal bridge between the high-thermal-conductivity sand grains than does methane gas [*Waite et al.*, 2002].

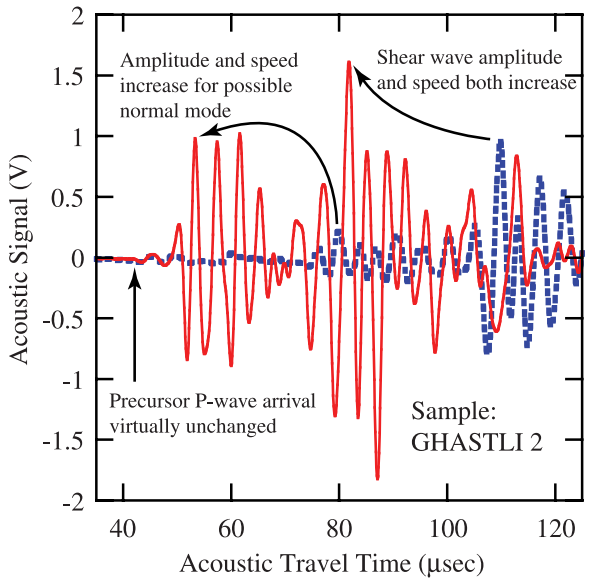

Figure 5. Hydrate redistribution resulting from a brief depressurization followed by repressurization changes certain aspects of the acoustic signal. The original shear wave arrival near 110 ms travel time (dotted blue curve) increases in amplitude by ~66% and travels 47% faster (solid red curve) as a result of the hydrate redistribution. A possible normal-mode feature initially arriving near 80 μs (M. Lee, personal communication, 2007) experiences a similar shift, but the small P wave arrival near 40 μs remains nearly unchanged.

[42] The 5.4% increase in thermal conductivity for a pore-space hydrate saturation, S_h, of ~20% is significantly less than the 13.8% increase observed for the $S_h \approx 34\%$ case (Table 2). The dependence on initial hydrate saturation likely reflects differences not only in the extent of the hydrate migration toward the sample's central axis, but also in the amount of new hydrate growth from pore water that became isolated from the methane gas and did not form hydrate during the initial hydrate synthesis.

[43] A second one-atmosphere transfer was carried out on both samples, causing an additional increase in λ. The effect was smaller than for the first cycle, resulting in an additional 3.6% increase for the low-hydrate-saturation sample and an additional 2.5% increase for the higher-hydrate-saturation sample. Hydrate redistribution following the first depressurization cycle reduces the hydrate saturation in the outer portions of the sample. Reducing the volume of hydrate near the outer surface of the sample, where hydrate is most susceptible to alteration from a brief depressurization, mutes the impact of a subsequent brief depressurization on the sample's physical properties.

[44] The impact of a one-atmosphere transfer on λ depends on the location at which λ is measured. If we had adopted a guarded-plate measurement scheme in which the sensor is placed on the sample surface rather than the interior [*Cook and Leaist*, 1983; *Taylor et al.*, 2007], our measurement sensitivity would have been highest in the zone of hydrate depletion. We would therefore have expected a decrease rather than increase in λ. The physical property variation with measurement location in a sample further complicates the estimation of in situ properties from property measurements of disturbed core material.

4.3. Effect on Acoustic Wave Speed Measurements

[45] As with thermal conductivity measurements, our acoustic measurements are most sensitive to changes occurring along the sample's central axis because of the central location of our transducers in their endcaps. Increasing the hydrate saturation along the sample's axis is expected to more effectively cement sand grains, stiffen the sample, and thereby increase the measured wave speed [*Dvorkin et al.*, 2000] in the central portion of the sample where the transducers are most sensitive. As the sample stiffens with increasing hydrate cementation of the sand grains, acoustic transmission should be more efficient, increasing the observed acoustic amplitude [*Waite et al.*, 2004].

[46] Figure 5 compares the acoustic signal produced by the shear wave crystals before and after the brief excursion from the hydrate stability field. Results from the higher of the two hydrate saturations tested are shown, but both samples display the same basic waveform changes: (1) acoustic travel times generally decrease, meaning the associated wave speeds increase, and (2) acoustic amplitudes generally increase, by 66% in the case of the shear wave shown in Figure 5.

[47] As noted in the CT results, hydrate forms rapidly following repressurization. Even just 3 h after repressurization, the waveform amplitude surpassed the predepressurizaton amplitude (blue curve in Figure 5). The waveform required only 3 days to fully develop and equilibrate following repressurization (red curve in Figure 5), as compared to the 14 days required for the initial waveform to grow and stabilize.

[48] As shown in Table 2, the P wave speed, V_p, for the GHASTLI 2 sample decreased by 2.4%. The correspondingly large 47% increase in shear wave speed, V_s, suggests hydrate redistribution and new hydrate growth significantly increased the grain-to-grain stiffness along the central axis of the sample. In the presence of free gas this stiffness increase could indicate enhanced intergranular cementation, but the corresponding P wave speed and amplitude increase [*Lee*, 2004] is not observed. An enhanced S wave speed response coupled with a muted P wave speed response to an increased hydrate saturation has been observed in laboratory studies of THF hydrate-bearing sand [*Yun et al.*, 2005]. *Yun et al.* [2005] show how such a response can be modeled assuming hydrate forms initially on the surface of grains, with subsequent growth into the pore space rather than at grain contacts. As discussed in section 5, an insensitivity of V_p to a brief depressurization has also been observed in naturally occurring, highly cemented sands [*Winters et al.*, 1999].

4.4. Effect on Shear-Strength Measurements

[49] The hydrate saturation increase along the sample axis resulting from a brief depressurization has the potential to stiffen the sample by strengthening bonds between sand grains, but that strengthening comes at the expense of cement lost from between grains near the sample perimeter during the brief depressurization. Despite changes in hydrate distribution, the average equilibrium concentration of

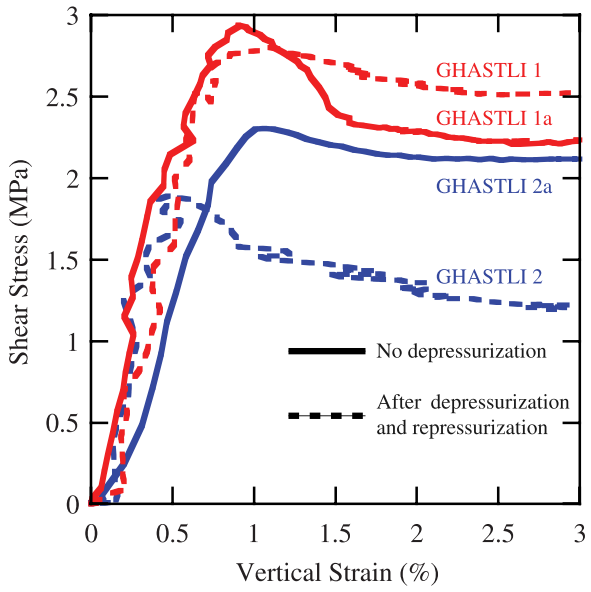

Figure 6. Triaxial shear testing for hydrate-cemented sands that have (dotted curves) and have not (solid curves) experienced a brief depressurization. A brief depressurization does not significantly alter the shear stress dependence on strain prior to shear but does reduce the peak shear stress. The stress drop following the peak stress does not correlate with whether samples have experienced a brief depressurization.

gas hydrate within any cross section may therefore be similar before and after a brief depressurization.

[50] Figure 6 compares the shear-strength response to axial strain in four different samples. The simulated one-atmosphere transfer appears to reduce the peak shear stress each sample can support, but even the peak stress decrease of 18% for the $S_h \approx 20\%$ case is within the expected sample-to-sample variation of ±15%.

[51] Other shear characteristics do not correlate with the effects of hydrate redistribution. Prior to failure, for instance, the slope of shear stress versus strain is nearly independent of hydrate saturation, in agreement with measurements on methane-hydrate-bearing sediment by *Hyodo et al.* [2005], and that slope does not change dramatically as a result of hydrate redistribution. The shear-stress decrease following the peak stress also does not correlate with the hydrate redistribution, becoming more pronounced for the $S_h \approx 20\%$ case, but less pronounced for the $S_h \approx 43\%$ case. On the basis of our study, the shear-strength measurement changes are not significantly correlated with effects of hydrate redistribution in cemented, gas-rich sand samples. This lack of correlation complicates the assessment of in situ shear properties based on measurements of briefly depressurized samples.

4.5. Hydrate Formation Controls on the Initial Physical Property Measurements

[52] In the same fashion that a brief depressurization induces water migration via capillary action within a sample, capillary action causes water to migrate within a sample during the initial hydrate formation procedure [*Kneafsey et al.*, 2007]. As shown in Figure 2, an initially uniform sample of partially water-saturated sand can form a slightly inhomogeneous hydrate-bearing sand. While it is possible that our higher-hydrate-saturation samples exhibit lower thermal conductivity and shear wave speed than their lower-hydrate-saturation counterparts because of differences in their formation-induced inhomogeneities, the inhomogeneities have not yet been quantified in terms of the extent to which they depend on initial water saturation, hydrate formation rate, and other factors.

5. Implications for Highly Hydrate-Saturated Sand

[53] The weak effect a brief depressurization has on V_p in our laboratory-formed, hydrate-bearing sands has also been observed in a hydrate-bearing sand sample recovered beneath permafrost at the Mallik 2L-38 site in the MacKenzie Delta region of the Canadian Northwest Territories [*Winters et al.*, 1999]. In spite of obvious differences in sample character and handling, the Mallik sample provides a link between our laboratory results and expectations for highly hydrate-saturated sands.

[54] The Mallik 2L-38 core contained pore-space hydrate saturations of 70–74% [*Lee and Collett*, 1999]. Collected as a conventional core, the sample was depressurized during its recovery from depth. The sample also froze during retrieval through the overlying permafrost. The sample was stored in a methane-pressurized vessel and kept frozen during transport to the GHASTLI facility. The sample was then depressurized briefly below the freezing temperature before being transferred into GHASTLI at room temperature.

[55] The core's transfer into GHASTLI is similar to the brief depressurization experienced by our laboratory-formed, hydrate-bearing sands. The Mallik sample was depressurized while it was frozen, which limits the hydrate dissociation rate [*Stern et al.*, 2001]. The sample partially thawed during the room temperature transition into GHASTLI, however [*Winters et al.*, 1999]. Similar to Figure 4, the sample was most susceptible to dissociation near its cylindrical surface prior to being repressurized into the methane-hydrate stability field. In spite of the potential for sample disturbance during retrieval, transport and transfer into GHASTLI, V_p for the Mallik 2L-38 core measured in GHASTLI was in agreement with downhole logging results [*Winters et al.*, 1999].

[56] A key similarity between our laboratory-formed, hydrate-cemented sands and the Mallik sample is the extent to which methane hydrate bonds sediment grains. Naturally occurring hydrate in sand is generally thought to be a load-bearing sediment component [*Kleinberg et al.*, 2005], rather than providing the strong intergranular bonding seen in out hydrate-cemented laboratory samples. Nevertheless, in laboratory studies of noncementing THF hydrate sediments with pore-space hydrate contents exceeding 50% appear to maintain intergranular bonding by hydrate during a reduction in effective stress, limiting the sample alteration during sample recovery as long as the sediment is returned to its in situ effective stress state prior to measuring the acoustic wave speeds [*Lee et al.*, 2008]. Pore-space hydrate saturations exceeding 50% in sands have been found not only at the Mallik site, but also beneath permafrost at the Mt. Elbert

site on the Alaskan North Slope [*Mount Elbert Science Team*, 2007], as well as in marine sands in the Nankai Trough offshore Japan [*Matsumoto*, 2002], and at the Tigershark well in the Gulf of Mexico [*Smith et al.*, 2006].

[57] Our laboratory technique, forming methane hydrate from partially water-saturated sands, cements sand grains with hydrate, providing strong intergranular bonding. Following the primary hydrate formation stage, V_p in the 43% hydrate saturation sample is 3430 m/s (see Table 2), more than triple the value for the partially water-saturated sand pack prior to hydrate formation [*Waite et al.*, 2004]. Even in our 20% hydrate saturation sample, V_p, changes by less than 5% in response to a brief depressurization. This resilience in V_p is not expected in noncementing hydrate cases for all hydrate saturation levels, however. For pore-space hydrate contents below ~40%, intergranular bonding by hydrate is less significant and effective stress changes can alter the sample [*Yun et al.*, 2007].

[58] An important difference between our laboratory samples and the Mallik 2L-38 core is the temperature during depressurization. Our laboratory samples were above freezing prior to depressurization, while the Mallik core was frozen. Depressurization below the freezing point preserves hydrate by lowering the dissociation rate [*Stern et al.*, 2001], but freezing also causes interstitial pore water to expand, potentially fracturing the sediment.

[59] In highly hydrate-saturated sands such as the Mallik 2L-38 sample, consistent V_p results from laboratory and downhole logging measurements [*Winters et al.*, 1999] imply pore water volumes were low enough that pore water freezing did not significantly alter the sample. Prior to depressurization, freezing high-hydrate-content sands even from marine environments may preserve hydrate without significantly altering the host sediment fabric. Lower hydrate-content sediments, however, may contain enough water that expansion due to pore water freezing does significantly disturb the host sediment fabric.

6. Implications for Water-Saturated, Methane Hydrate-Bearing Sediment

[60] A critical difference between the gas-rich, hydrate-bearing sand samples discussed above and water-saturated hydrate-bearing core recovered in the field is the extent to which gas produced during a brief depressurization escapes the sample. Our gas-rich, hydrate-bearing sands were permeable, containing gas-filled pathways through which gas produced via hydrate dissociation could escape the sample during depressurization. In water-saturated sediment, particularly fine-grained sediment, such vent pathways are restricted. These restrictions lead to bubble formation and effective stress reduction [*Yun et al.*, 2006], both of which are exacerbated by methane-hydrate dissociation. As discussed below, bubble formation and effective stress reduction, combined with hydrate redistribution, can lead to physical property changes that vary from sample to sample and are therefore difficult to correct for.

6.1. Bubble Formation

[61] Depressurizing water-saturated, hydrate-bearing sediment draws gas dissolved in the pore water out of solution in addition to producing gas via hydrate dissociation. Repressurization can force gas back into the dissolved phase, but the maximum quantity of dissolved gas is limited by the gas's solubility in water. In a sample containing gas produced from hydrate dissociation, the solubility limit can be exceeded, allowing hydrate-forming gas to remain in the gas phase immediately following repressurization. The persistence of gas bubbles following pressurization can lead to hydrate formation, because the bubble's gas-water interface provides an efficient hydrate growth surface [*Freer et al.*, 2001]. Because bubble location and volume depend on the sample's lithology, pore water methane saturation, and hydrate content, hydrate formed from bubbles will be distributed according to those sample-dependent characteristics. As shown in our laboratory samples, hydrate redistribution can alter the sample's physical properties.

[62] Bubble growth itself can alter a sample's physical properties, attenuating compressional waves and reducing the measured wave speed relative to in situ values. The magnitude of the change depends on the extent of bubble formation, which itself depends on the sample's lithology, pore water methane saturation, and hydrate content. Although hydrate dissociation can significantly increase the amount of free gas produced as a result of core depressurizaton, bubble growth is a concern for any water-saturated core with dissolved gas, regardless of whether hydrate is present.

[63] By maintaining near in situ hydrostatic pressure throughout the core-acquisition and property-measurement process, bubble formation and hydrate redistribution can be curtailed. Compressional wave speed measurements made using the Instrumented Pressure Testing Chamber (IPTC) on clay-rich Gulf of Mexico sediment recovered and measured while maintaining near in situ pressure are only 2% below the logging while drilling (LWD) results [*Yun et al.*, 2006].

6.2. Loss of Effective Stress

[64] Although current pressure-coring technology is able to preserve near-in situ hydrostatic pressure, the effective stress pushing sediment grains against each other is not maintained. Particularly in fine-grained sediment, bubble formation caused by hydrate dissociation can increase the pore pressure, further reducing the effective stress [*Xu and Germanovich*, 2006], weakening grain-to-grain contacts and reducing the sediment frame stiffness [*Francisca et al.*, 2005]. As a result, the compressional and shear wave speeds as well as the sediment strength are all reduced [*Yun et al.*, 2006]. As described above, bubble formation varies from sample to sample, complicating efforts to predict or account for the ensuing degradation of the matrix stiffness. By maintaining the hydrostatic pressure, however, pressure coring can avoid the additional matrix weakening caused by bubble formation and expansion.

7. Conclusion

[65] We have shown that in gas-rich, laboratory-formed methane-hydrate-cemented sands, even a brief depressurization to one atmosphere induces hydrate redistribution within the sample. This redistribution creates a sample with new physical properties that can differ significantly from those of the original sample. Measured changes depend on

whether a given property is measured near the sample perimeter, which loses hydrate during the simulated core transfer, or near the sample center, which gains hydrate. Briefly dropping the pressure to one atmosphere a second time, to simulate the transfer of core from a storage vessel into a laboratory measurement apparatus, leads to continued hydrate redistribution, though to a lesser extent than the initial simulated transfer.

[66] Estimating in situ properties from initially water-saturated recovered core that has experienced a depressurization cycle is further complicated by bubble formation and loss of effective stress, with hydrate dissociation exacerbating both processes. Property changes therefore vary not only on the basis of which portion of the sample is being measured, but on sample-to-sample differences in initial hydrate saturation and lithology. Unpredictable location- and sample-dependent property changes complicate the assessment of in situ properties based on recovered core material. Accurate in situ property estimates from recovered cores require careful preservation of the in situ stress state throughout the recovery and measurement process, even in non-hydrate-bearing material.

[67] **Acknowledgments.** This work benefited from discussions with C. Santamarina, T.-S. Yun, and C. Ruppel, with reviews by M. Kowalsky and D. Hawkes greatly improving the quality of this manuscript. U. S. Geological Survey contributions were supported by the Gas Hydrate Project of the U. S. Geological Survey's Coastal and Marine Geology Program, in addition to Department of Energy contract DE-AI21-92MC29214. CT scanning at the Lawrence Berkeley National Laboratory was artfully performed by L. Tomutsa and supported by the Assistant Secretary for Fossil Energy, Office of Oil and Natural Gas, through the National Energy Technology Laboratory of the U. S. Department of Energy under contract DE-AC02-05CH11231.

References

Bohrmann, G., J. Greinert, E. Suess, and M. Torres (1998), Authigenic carbonates from the Cascadia subduction zone and their relation to gas hydrate stability, *Geology*, *26*, 647–650.

Bowles, J. E. (1979), *Physical and Geotechnical Properties of Soils*, 478 pp., McGraw-Hill, New York.

Collett, T. S., M. Riedel, R. Boswell, J. R. Cochran, P. Kumar, A. K. Sethi, A. V. Sathe, and N. E.-S. Party (2006), International team completes landmark gas hydrate expedition in the offshore of India, in *Fire in the Ice*: *Methane Hydrate Newsletter*, *Fall 2006*, pp. 1–4, Natl. Energy Technol. Lab., U. S. Dept. of Energy, Morgantown, W. Va.

Cook, J. G., and D. G. Leaist (1983), An exploratory study of the thermal conductivity of methane hydrates, *Geophys. Res. Lett.*, *10*, 397–399.

Dvorkin, J., M. B. Helgerud, W. F. Waite, S. H. Kirby, and A. Nur (2000), Introduction to physical properties and elasticity models, in *Natural Gas Hydrate in Oceanic and Permafrost Environments*, edited by M. D. Max, pp. 245–260, Springer, New York.

Expedition 311 Scientists (2006), Site U1327, in *Proceedings of the Integrated Ocean Drilling Program*, vol. 311, edited by M. Riedel et al., Integrated Ocean Drill. Program Manage. Int., Inc., Washington, D.C., doi:10.2204/iodp.proc.311.105.2006.

Francisca, F., T. S. Yun, C. Ruppel, and J. C. Santamarina (2005), Geophysical and geotechnical properties of near-seafloor sediments in the northern Gulf of Mexico gas hydrate province, *Earth Planet. Sci. Lett.*, *237*, 924–939.

Freer, E. M., M. Sami Selim, and E. D. Sloan (2001), Methane hydrate film growth kinetics, *Fluid Phase Equilibria*, *185*, 65–75.

Guerin, G., and D. Goldberg (2005), Modeling of acoustic wave dissipation in gas hydrate-bearing sediments, *Geochem. Geophys. Geosyst.*, *6*, Q07010, doi:10.1029/2005GC000918.

Guerin, G., D. Goldberg, and A. Meltser (1999), Characterization of in situ elastic properties of gas hydrate-bearing sediments on the Blake Ridge, *J. Geophys. Res.*, *104*, 17,781–17,795.

Gupta, A., T. J. Kneafsey, G. J. Moridis, Y. Seol, M. B. Kowalsky, and E. D. Sloan (2006), Methane hydrate thermal conductivity in a large heterogeneous porous sample, *J. Phys. Chem. B*, *11*, 16,384–16,392, doi:10.1021/jp0619639.

Helgerud, M. B., J. Dvorkin, A. Nur, A. Sakai, and T. Collett (1999), Elastic-wave velocity in marine sediments with gas hydrates: Effective medium modeling, *Geophys. Res. Lett.*, *26*, 2021–2024.

Hovland, M., and O. T. Gudmestad (2001), Potential influence of gas hydrate on seabed installations, in *Natural Gas Hydrates: Occurrence, Distribution, and Detection*, *Geophys. Monogr. Ser.*, vol. 124, edited by C. K. Paull and W. P. Dillon, pp. 307–315, AGU, Washington, D. C.

Hyodo, M., Y. Nakata, N. Yoshimoto, and T. Ebinuma (2005), Basic research on the mechanical behavior of methane hydrate-sediments mixture, *Soils Found.*, *45*(1), 75–85.

Kerr, R. A. (2004), Gas hydrate resource: Smaller but sooner, *Science*, *303*, 946–947.

Kleinberg, R. L., C. Flaum, and T. S. Collett (2005), Magnetic resonance log of JAPEX/JNOC/GSC et al. Mallik 5L-38 gas hydrate production research well: Gas hydrate saturation, growth habit, relative permeability, in *Scientific Results From the Mallik 2002 Gas Hydrate Production Research Well Program, Makenzie Delta, Northwest Territories, Canada*, edited by S. R. Dallimore and T. S. Collett, *Bull. Geol. Surv. Can.*, 585, 10 pp.

Kneafsey, T. J., L. Tomutsa, G. J. Moridis, Y. Seol, B. M. Freifeld, C. E. Taylor, and A. Gupta (2007), Methane hydrate formation and dissociation in a partially saturated core-scale sand sample, *J. Pet. Sci. Eng.*, *56*, 108–126.

Kvenvolden, K. A. (1993), Gas hydrates: Geological perspective and global change, *Rev. Geophys.*, *31*, 173–187.

Kvenvolden, K. A., and T. D. Lorenson (2001), The global occurrence of natural gas hydrates, in *Natural Gas Hydrates: Occurrence, Distribution, and Detection*, *Geophys. Monogr. Ser.*, vol. 124, edited by C. K. Paull and W. P. Dillon, pp. 3–18, AGU, Washington, D. C.

Lee, J.-Y., J. C. Santamarina, and C. Ruppel (2008), Mechanical and electromagnetic properties of northern Gulf of Mexico sediments with and without THF hydrates, *Mar. Pet. Geol.*, *25*, doi:10.1016/j.marpetgeo.2008.01.019, in press.

Lee, M. W. (2004), Elastic velocities of partially gas-saturated unconsolidated sediments, *Mar. Pet. Geol.*, *21*, 641–650.

Lee, M. W., and T. Collett (1999), Amount of gas hydrate estimated from compressional-and shear-wave velocities at the JPEX/JNOC/GSC Mallik 2L-38 gas hydrate research well, *Bull. Geol. Surv. Can.*, *544*, 313–322.

Lee, M. W., and T. S. Collett (2005), Assessments of gas hydrate concentrations estimated from sonic logs in the JAPEX/JNOC/GSC et al. Mallik 5L-38 gas hydrate research production well, in *Scientific Results From the Mallik 2002 Gas Hydrate Production Research Well Program, Makenzie Delta, Northwest Territories, Canada*, edited by S. R. Dallimore and T. S. Collett, *Bull. Geol. Surv. Can.*, 585, 10 pp.

Leg 204 Shipboard Scientific Party (2003), Explanatory notes, *Proc. Ocean Drill. Program Initial Rep.*, 204, 1–102.

Matsumoto, R. (2002), Comparison of marine and permafrost gas hydrates: Examples from Nankai Trough and Mackenzie Delta, paper presented at 4th International Conference on Gas Hydrates, Heat Transfer Soc. of Japan, Yokohama, Japan, 19–23 May.

Moridis, G. J., and M. B. Kowalsky (2006), Response of oceanic hydrate-bearing sediments to thermal stresses, paper 18193 presented at Offshore Technology Conference, Am. Assoc. of Pet. Geol., Houston, Tex., 1–4 May.

Mount Elbert Science Team (2007), Alaska North Slope well successfully cores, logs, and tests gas-hydrate-bearing reservoirs, in *Fire in the Ice: Methane Hydrate Newsletter, Winter 2007*, pp. 1–4, Natl. Energy Technol. Lab., U.S. Dept. of Energy, Morgantown, W. Va.

Nixon, M. F., and J. L. H. Grozic (2007), Submarine slope failure due to gas hydrate dissociation: A preliminary quantification, *Can. Geotech. J.*, *44*, 314–325.

Osegovic, J. P., S. R. Tatro, and S. A. Holman (2006), Physical chemical characteristics of natural gas hydrate, in *Economic Geology of Natural Gas Hydrate*, edited by M. D. Max et al., pp. 45–104, Springer, New York.

Paull, C. K., W. Ussler, and W. P. Dillon (2000), Potential role of gas hydrate decomposition in generating submarine slope failures, in *Natural Gas Hydrate in Oceanic and Permafrost Environments*, edited by M. D. Max, pp. 149–156, Springer, New York.

Ruppel, C. (2007), Tapping methane hydrates for unconventional natural gas, *Elements*, *3*, 193–199.

Smith, S., R. Boswell, T. Collett, M. Lee, and E. Jones (2006), Alaminos Canyon Block 818: A documented example of gas hydrate saturated sand in the Gulf of Mexico, in *Fire in the Ice: Methane Hydrate Newsletter, Fall 2006,* pp. 12–13, Natl. Energy Technol. Lab., U. S. Dept. of Energy, Morgantown, W. Va.

Stern, L. A., S. Circone, S. H. Kirby, and W. B. Durham (2001), Anomalous preservation of pure methane hydrate at 1 atm, *J. Phys. Chem. B*, *105*, 1756–1762.

Taylor, C. E., D. D. Link, and N. English (2007), Methane hydrate research at NETL: Research to make methane production from hydrates a reality, *J. Pet. Sci. Eng.*, *56*, 186–191.

Vargaftik, N. B., L. P. Filippov, A. A. Tarzimanov, and E. E. Totskii (1993), *Handbook of Thermal Conductivity of Liquids and Gases*, CRC Press, Boca Raton, Fla.

Waite, W. F., B. J. deMartin, S. H. Kirby, J. Pinkston, and C. D. Ruppel (2002), Thermal conductivity measurements in porous mixtures of methane hydrate and quartz sand, *Geophys. Res. Lett.*, *29*(4), 2229, doi:10.1029/2002GL015988.

Waite, W. F., W. J. Winters, and D. H. Mason (2004), Methane hydrate formation in partially water-saturated Ottawa sand, *Am. Mineral.*, *89*, 1202–1207.

Waite, W. F., L. Y. Gilbert, W. J. Winters, and D. H. Mason (2006), Estimating thermal diffusivity and specific heat from needle probe thermal conductivity data, *Rev. Sci. Instrum.*, *77*, 044904, doi:10.1063/1.2194481.

Waite, W. F., L. A. Stern, S. H. Kirby, W. J. Winters, and D. H. Mason (2007), Simultaneous determination of thermal conductivity, thermal diffusivity and specific heat in sI methane hydrate, *Geophys. J. Int.*, *169*, 767–774, doi:10.1111/j.1365-246X.2007.03382.x.

Winters, W. J., I. A. Pecher, J. S. Booth, D. H. Mason, M. K. Relle, and W. P. Dillon (1999), Properties of samples containing natural gas hydrate from Mallik using GHASTLI, *Bull. Geol. Surv. Can.*, *544*, 241–250.

Winters, W. J., W. P. Dillon, I. A. Pecher, and D. H. Mason (2000), GHASTLI: Determining physical properties of sediment containing natural and laboratory-formed gas hydrate, in *Natural Gas Hydrate in Oceanic and Permafrost Environments*, edited by M.D. Max, pp. 311–322, Springer, New York.

Winters, W. J., W. F. Waite, D. R. Hutchinson, and D. H. Mason (2005), Physical property studies in the USGS GHASTLI laboratory, in *Fire in the Ice: Methane Hydrate Newsletter, Fall 2005*, pp. 6–9, Natl. Energy Technol. Lab., U. S. Dept. of Energy, Morgantown, W. Va.

Xu, W., and L. N. Germanovich (2006), Excess pore pressure resulting from methane hydrate dissociation in marine sediments: A theoretical approach, *J. Geophys. Res.*, *111*, B01104, doi:10.1029/2004JB003600.

Yuan, T., G. D. Spence, R. D. Hyndman, T. A. Minshull, and S. C. Singh (1999), Seismic velocity studies of a gas hydrate bottom-simulating reflector on the northern Cascadia continental margin: Amplitude modeling and full waveform inversion, *J. Geophys. Res.*, *104*, 1179–1191.

Yun, T. S., F. M. Francisca, J. C. Santamarina, and C. Ruppel (2005), Compressional and shear wave velocities in uncemented sediment containing gas hydrate, *Geophys. Res. Lett.*, *32*, L10609, doi:10.1029/2005GL022607.

Yun, T. S., G. A. Narsilio, J. C. Santamarina, and C. Ruppel (2006), Instrumented pressure testing chamber for characterizing sediment cores recovered at in situ hydrostatic pressure, *Mar. Geol.*, *229*, 285–293.

Yun, T. S., J. C. Santamarina, and C. Ruppel (2007), Mechanical properties of sand, silt, and clay containing tetrahydrofuran hydrate, *J. Geophys. Res.*, *112*, B04106, doi:10.1029/2006JB004484.

T. J. Kneafsey, Lawrence Berkeley National Laboratory, 1 Cyclotron Rd., MS 90R1116, Berkeley, CA 94720, USA.

D. H. Mason, W. F. Waite, and W. J. Winters, U. S. Geological Survey, 384 Woods Hole Road, Woods Hole, MA 02543, USA. (wwaite@usgs.gov)